Original scientific paper

Elevated temperature erosion of abradable seal coating

Bharti Malvi[1],✉ and Manish Roy[2]

[1]*National Institute of Technology, Jamshedpur: 831014, India*
[2]*Defence Metallurgical Research Laboratory, PO: Kanchanbagh, Hyderabad, 500 058, India*
Corresponding author: ✉*bharti.malvi@gmail.com*

Abstract

Abradable coatings are essentially sealing materials and are deposited by thermal spray techniques. The main function of these coatings is to control the clearance of the gas path of the gas turbine engines. The abradable coating prevents turbine blade damage by abrading itself when there is an offset or vibration during turbine operation. Since the coating is meant to abrade, the preferred coating material is relatively softer than the turbine blade material. As these coatings are prone to solid particle erosion at high temperatures, the erosion response of these coatings at elevated temperatures needs to be investigated. In order to achieve this objective, MCrAlY boron nitride polymer coating was deposited employing an air plasma spraying technique on a Ni-base alloy substrate. The important features of the microstructure and mechanical properties of the coating were examined, and the coating was subjected to erosion at various temperatures under different erosion conditions. The results indicate a ductile erosion behaviour for an abradable top coat. The erosion rate increases with the temperature of the coating. The detailed results of the investigation are presented, and the erosion mechanisms are studied.

Keywords

Abradable coating, high-temperature erosion, erosive wear, plasma spraying technique, mass-loss

Introduction

Deposition of abradable coating by thermal spraying has revolutionized the sealing technology of turbomachinery [1]. In order to ensure enhanced engine efficiency, the clearance between the static and the rotating parts should be minimized. Abradable coatings are employed in turbomachinery to reduce leakage gaps between stationary and rotating parts and control the clearance between the blade tip and casing in the turbines. Shaft labyrinth seal, shrouded blade labyrinth seal, and unshrouded labyrinth blade seal are three important labyrinth seals of gas turbine engines. Abradable coatings employed for sealing turbomachinery should exhibit not only resistance to various high-temperature corrosions and high cohesive strength but also should be resistant to solid particle erosion.

Thermal spraying is an important technique for depositing various coatings [2,3]. Abradable coatings are deposited using flame spray, atmospheric plasma spray (APS) technique, and high-

velocity oxy-fuel (HVOF) technique. Coatings such as aluminum polymer, aluminum boron nitride, and aluminum bronze polymers deposited by APS are used for relatively low-temperature applications. Zirconia-based ceramic abradable coatings used for a temperature around 1100 °C are another variety of plasma sprayed coating. MCrAlY boron nitrite polymer coatings are developed and deposited by plasma spraying for intermediate temperatures ranging from 700 to 850 °C. This coating is harder than low-temperature coatings, and abradability is controlled by porosity content, while boron nitrite provides lubricating action. The quantity of porosities in this coating is controlled by post-coating heat treatment.

Abradable coatings are subjected to various types of degradation such as high-temperature corrosion [4], thermal shock [5], erosion at room and elevated temperature [6], *etc.* Erosion is characterized by continuous material removal from eroding surfaces because of repeated impingement by erodent [6]. Elevated temperature erosive wear is a result of simultaneous degradation due to the impact of solid particles and oxidation [7]. It is also an important degradation process for MCrAlY boron nitrite polymer abradable coatings. Erosion of abradable coating is already reported in the literature by several investigators [8–10]. Kumar *et al.* [11] studied erosion Al-Si polyester abradable coatings sprayed by HVOF at 25, 200 and 400 °C temperatures and at 30, 60 and 75° impact angles. They found erosion rate is maximum at an intermediate impact angle. An investigation by Siddiqui *et al.* [9] with CoNiCrAlY with polyester and BN coating indicated that the average erosion rate is 0.22 (mm/s) (seconds/mil). Maozhong *et al.* [8] examined erosion of coatings having 75 % Ni +25 % graphite, 57 % Al + 8 % Si + 35 % graphite, 40 % Al + 5.5 % Si + 45.5 % graphite + 9 % organic binder and 40 % polyester + 60 % Al–Si alloy deposited by plasma spray method. They reported that the maximum erosion occurred at a 60° angle of impact. Erosion occurs by tunneling via pores and non-metal phase, micro-cutting, and plowing at oblique impact. The particles impact extrudes and produces indentations and extruded lips. These lips work-harden and eventually fall off. Maximum erosion rate at 60° impact angle is also reported by Sharsar *et al.* [10] for Al-Si polyester powders sprayed on titanium substrates by HVOF.

The above discussion clearly brings out the fact that although erosion is an important degradation process for abradable coating, erosion of abradable coating, particularly at elevated temperatures, has not been investigated comprehensively. The influence of temperature, impact angle, and impact velocity on erosion rate has not been reported. The influence of eroding conditions on the erosion behavior of MCrAlY boron nitrite polymer coatings at various temperatures is not available in the literature. Thus, the main objective of the proposed investigation is to evaluate the erosion response of MCrAlY boron nitrite polymer abradable coatings as a function of test conditions.

Experimental

Substrate and coating powder material

Ni-Cr alloy is taken as substrate material for abradable coatings. The Ni-Cr alloy was cut into pieces of 30×30×5 mm dimensions with the help of EDM. The specimens were subjected to sandblasting followed by ultrasonic cleaning in acetone prior to the coating deposition by plasma spraying. The characteristics of feedstock powder are listed in Table 1. SEM images showing the morphologies of the powders used for depositing bond coat and abradable coatings are shown in Figure 1. The powders for the bond coats are of high purity, spherical and dense. In contrast, powders of the abradable layer are spheroidal with different morphologies. The bond coat was essentially a CoNiCrAlY layer, and the composition of the bond coat was 38.5 wt.% Co, 32wt.%Ni, 21 wt.% Cr, 8 wt.% Al and 0.5 wt.% Y. Bond coat was about 100 μm thick.

Table 1. Feedstock powders used for abradable coating

Coating type-	Abradable coating	
Purpose	Bond coat	Top coat
Coating thickness	100μm	500μm
Designation	Amdry 961 (NiCrAlY)	Metco 2043 (CoNiCrAlY BN Polyester)
Chemical composition	Ni 22Cr 10Al 1.0Y	30Co 25Ni 16Cr 6Al 0.3Y 4BN 15Polyester
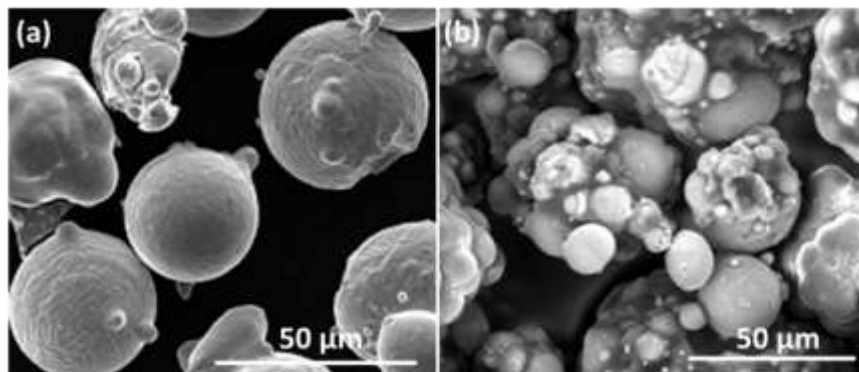
Figure 1. *SEM images showing morphologies of the powders used for depositing bond and abradable coating*

Deposition of coatings on substrates

The abradable coatings were deposited on Ni-Cr alloy substrates using an APS unit. The test specimens were held in a jaw for coating deposition immediately after sandblasting. The 9 MB plasma gun was operated at 590 amp to deposit coating material in powder form. Argon (carrier gas), argon (plasma arc), and hydrogen (secondary gas) were allowed to flow through the plasma gun. The plasma plume was formed by striking the arc with the gas molecules. Huge thermal energy was released as plasma ions returned to the gaseous state. The coating powders were fed into a gas plume. The powders were melted in the plume and propelled towards the substrate material to form the coating. The air plasma spray parameters used to coat abradable layers are listed in Table 2.

Table 2. Plasma spray conditions used for deposition of powders

Plasma spray parameters	Amdry 961 (NiCrAlY)	Metco 2043 (CoNiCrAlY BN Polyester)
Plasma arc current, A	450	450
Arc voltage, V	61.3	61.3
Plasma gas (Ar) flow rate, m^3s^{-1}	63.3E-5	63.3E-538
Secondary gas (H_2) flow rate, m^3s^{-1}	5.0E-5	5.0E-53
Carrier gas (Ar) flow rate, m^3s^{-1}	5.0E-5	5.0E-53
Stirrer rotation, rotation min^{-1}	30	30
Torch to base distance (TBD), mm	100	100

Erosion testing

Elevated temperature erosion was performed by employing a solid particle erosion test rig shown in Figure 2 [12]. The test facility was fabricated in a defense metallurgical research laboratory. The rig can conduct erosion tests at temperatures up to 1073 K with the combination of a wide range of parameters affecting erosion. The rig is equipped with two furnaces for heating the specimen and the air. The temperatures of the specimen and the furnace were regulated with the help of a controller setup and thermocouples. A miniature conveyer belt was employed at the bottom of the particle feeding hopper to control the particle feed rate. The impact velocity is monitored by varying the incoming air pressure by a pressure valve. Further detail of the test rig is available elsewhere [12].
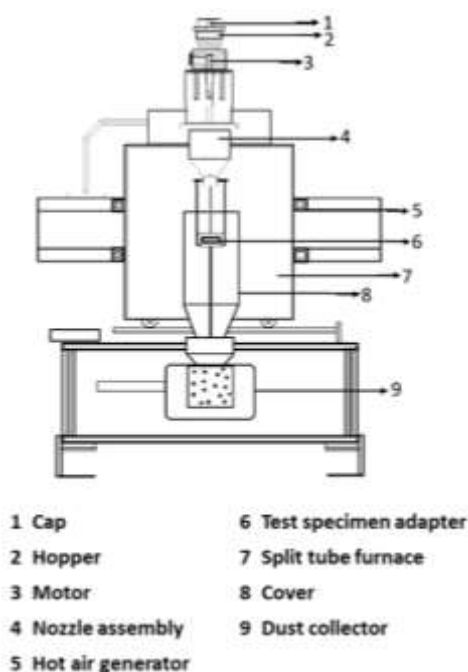
1	Cap	6	Test specimen adapter
2	Hopper	7	Split tube furnace
3	Motor	8	Cover
4	Nozzle assembly	9	Dust collector
5	Hot air generator		

Figure 2. Schematic diagram of high-temperature erosion rig

Impinging particles from the hopper were fed at a constant predetermined feed rate and were fluidized by dry compressed air. The particle-entrained air mixture was then accelerated through a nozzle of a diameter of 8 mm, and it was made to impinge on the test sample placed at a distance of 10 cm from the end of the nozzle. The impact angle was varied by changing the sample holders whose inclinations vary with respect to impacting air particle stream. Air pressure and erodent feed rate were regulated by the valves provided. The rotating disc method was used to determine the velocity of the erodent particles [13]. Ni substrates coated with an abradable layer were subjected to impingement by gas-laden particles at various temperatures. After exposure to a predetermined time, the samples were ultrasonically cleaned with acetone, dried, and then weighed in an electronic balance having precision up to 0.1 mg. Erosion test conditions are summarized in Table 3. An established test procedure was followed for each erosion test up to 673 K. The cleaned samples were weighed first and then subjected to erosion in the test rig for 5 minutes. The eroded specimen was weighed again to estimate the mass loss. This erosion is carried out 6 times or 30 minutes by weighing every 5 minutes. The ratio of mass loss suffered to the mass of the particles causing the mass loss gives the dimensionless erosion rate E. This procedure was repeated until a steady-state erosion rate was obtained. Further details of test techniques are available elsewhere [14].

Table 3. Erosion test conditions

Test variable	Test conditions
Erodent	SiO_2
Erodent size	150 ± 50 μm
Erodent shape	angular
Velocity	Low 57, high 93 m / s
Erodent feed rate	2.0 g / min
Angle of impingement	30 and 90º
Temperatures	Room temperature, 200, 400 and 600 °C
Sample size	30 ×30×5 mm
Exposure time	5 min

Examination of eroded surfaces

Eroded samples were examined under an environmental scanning electron microscope (ESEM) equipped with an energy dispersive spectroscopy (EDS) facility operating at 20 kV after cleaning the samples ultrasonically. Transverse sections of eroded samples were analyzed after polishing the cross-sections metallographycally. Samples were embedded into resin using a hot mounting technique for metallographic preparation. The demolition of the porous structure during sample preparation due to grinding, cutting, and polishing, etc., was avoided by infiltrating the porous coating with epoxy adhesives. The porosity of the porous coating was measured by image analysis.

Results and discussion

Microstructure of abradable coating

The XRD pattern of the abradable coating surface is illustrated in Figure 3. In addition to h-BN and γ-Co-Ni-Cr, the coating contains γ'Ni$_3$Al and βNiAl. Thus, there is no perceptible change in phases as a result of spraying. γ-Co-Ni-Cr and γ'Ni$_3$Al phases exhibit high intensity. The as-sprayed microstructure of the abradable coating is shown in Figure 4. The microstructure presented in Figure 4 shows that the ductility agents such as a polymer which provides friability, and h-BN, which acts as a lubricant, are homogeneously distributed in the coating, and there is no segregation of these phases in the microstructure.
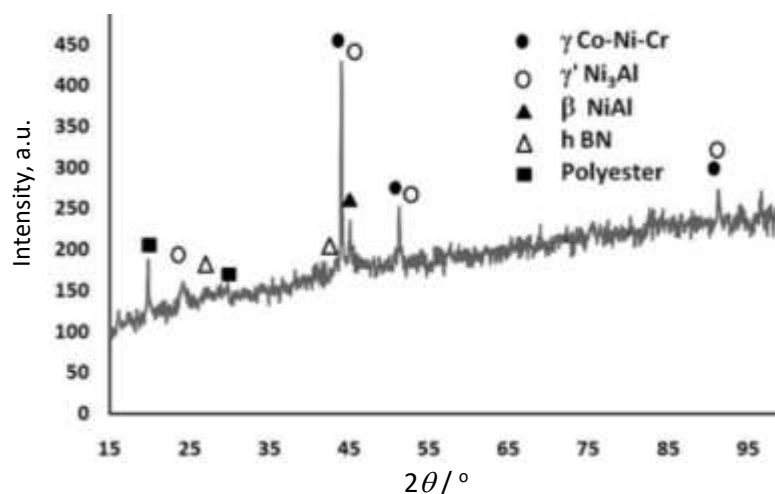

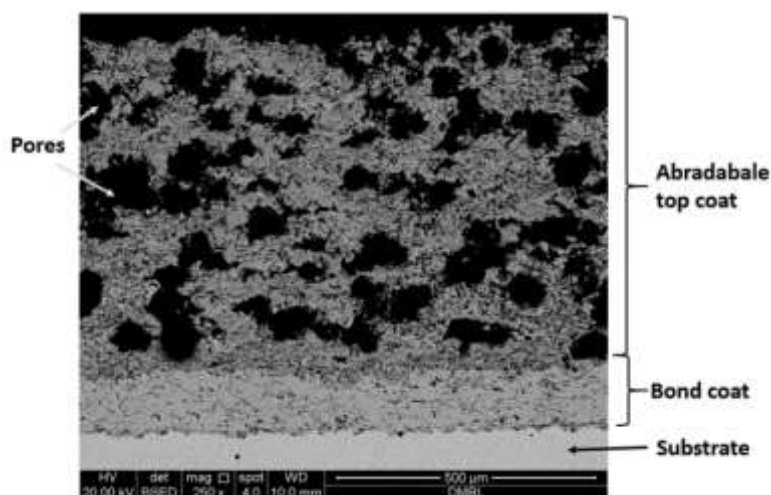**Figure 3.** *X-ray diffraction pattern of the abradable coating*

Figure 4. *SEM image showing the cross-section of the MCrAlY boron nitrite polymer abradable coating*

This segregation may be detrimental to the performance of the coatings. The microstructure was uniform in various regions of the sample and in different samples. The thickness of the NiCrAlY bond coat and CoNiCrAlY BN polyester topcoat are 100 μm and 650 μm approximately. To serve the purpose of abradability, the coating has a porous structure. The powders for their respective coatings were selected on the basis of their compatibility with the Ni-Cr substrate. The purpose of the abradable coating is to abrade off while rubbing, but at the same time, it should be erosion resistant. Abradability and erosion resistance are two contradictory phenomena. Hence, a compromise between them has to be made. In other words, abradability is governed by soft phases such as polyester and h-BN. In contrast, hard metallic phases such as γ-Co-Ni-Cr, $\gamma'Ni_3Al$ and $\beta NiAl$ determine erosion resistance. Thus, the microstructure is optimized to ensure good abradable behavior and erosion resistance.

Elevated temperature erosion of the abradable coating

Variations of incremental erosion rate as a function of the cumulative mass of the erodent at ambient and elevated temperature are illustrated in Figure 5 and Figure 6, respectively. Incremental erosion rate is presented under normal and oblique impact at two different impact velocities. Under all conditions, a steady-state erosion rate is attained from an initial high value. The highest erosion rate is obtained as expected under normal impact at an impact velocity of 93 m/s. The erosion rate at a higher temperature is higher than at an ambient or lower temperature.
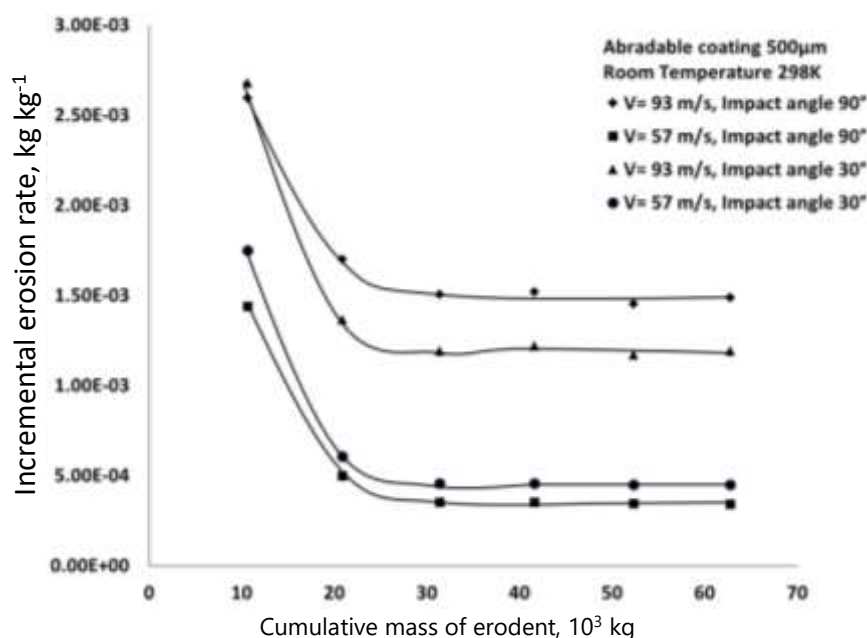

Figure 5. *Variations of incremental erosion rate as a function of the cumulative mass of the erodent at ambient temperature under normal and oblique impact at two different impact velocities*

The influence of test temperatures on the steady-state erosion rate of the abradable coating is presented in Figure 7. The erosion response is ductile, signifying a higher erosion rate at oblique impact at lower impact velocity and all temperatures. In contrast, a brittle erosion behavior at lower test temperature and ductile erosion response at a higher temperature at high impact velocity can be noted. Such difference in erosion behavior can be attributed to the deformation condition of the thermal sprayed coating during erosion [15] and the presence of porosities in abradable coatings, which contain around 12-18 % porosities.
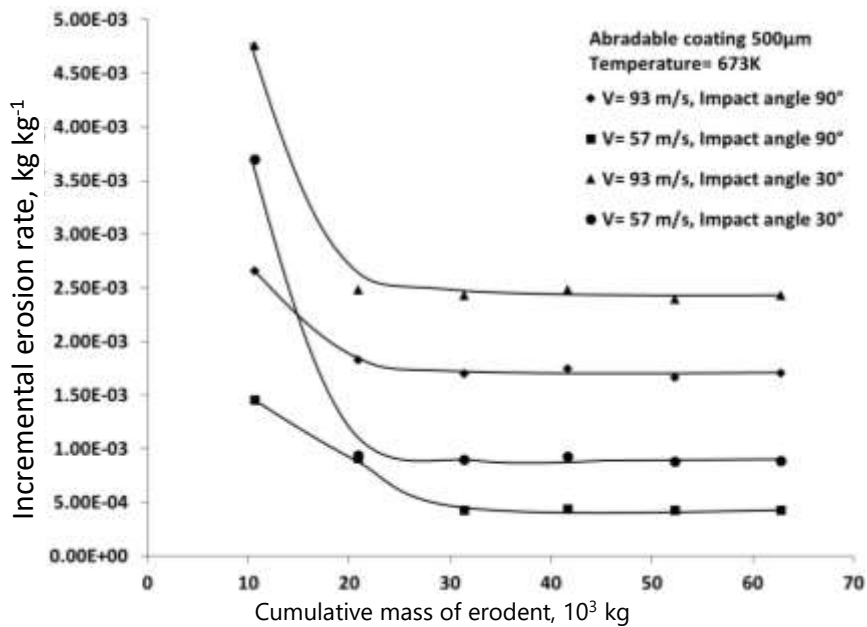
Figure 6. *Variations of incremental erosion rate as a function of the cumulative mass of the erodent at 673 K under normal and oblique impact at two different impact velocities*

It has been shown in earlier publications [16] that the strain rate associated with impact is directly proportional to the square root of impact velocity. Thus, the strain rate at higher impact velocity is higher than that at lower impact velocity. It is also noted that the strength of metallic materials increases, and the ductility decreases with an increase in strain rate. This increase in strength and decrease in ductility is more pronounced for a porous material. Thus, at low impact velocity, porous abradable MCrAlY boron nitrite polymer coatings exhibit brittle behavior and become ductile with an increase of strain rate at high impact velocity.
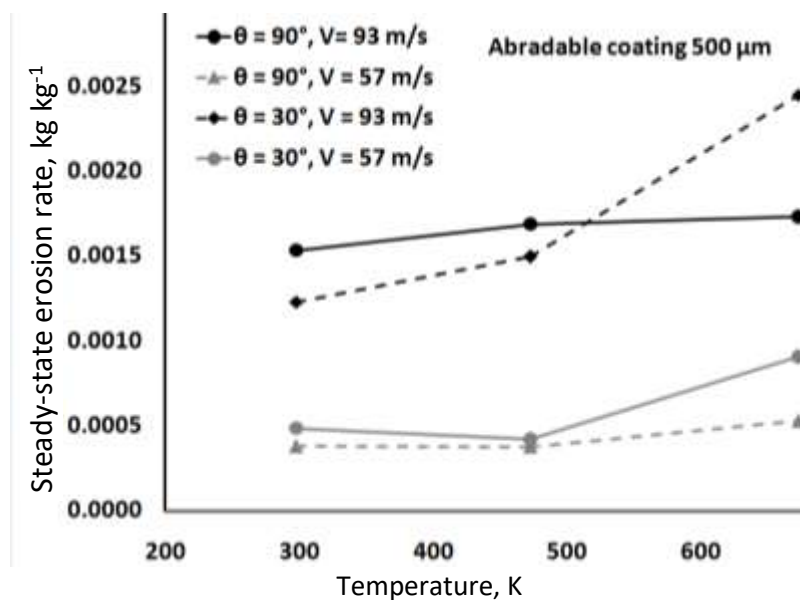

Figure 7. *The influence of test temperature on the steady-state erosion rate of the abradable coating*

The influence of impact velocity on erosion rate is characterized by velocity exponent n and is given by equation (1)

$$E_r = KV^n \tag{1}$$

where E_r is erosion rate, V is impact velocity, n is velocity exponent and K is a constant. The variation of velocity exponent n calculated for abradable coating as a function of test temperatures is furnished in Figure 8. Velocity exponents are between 2 to 3 and are generally indicative of ductile erosion response [17].
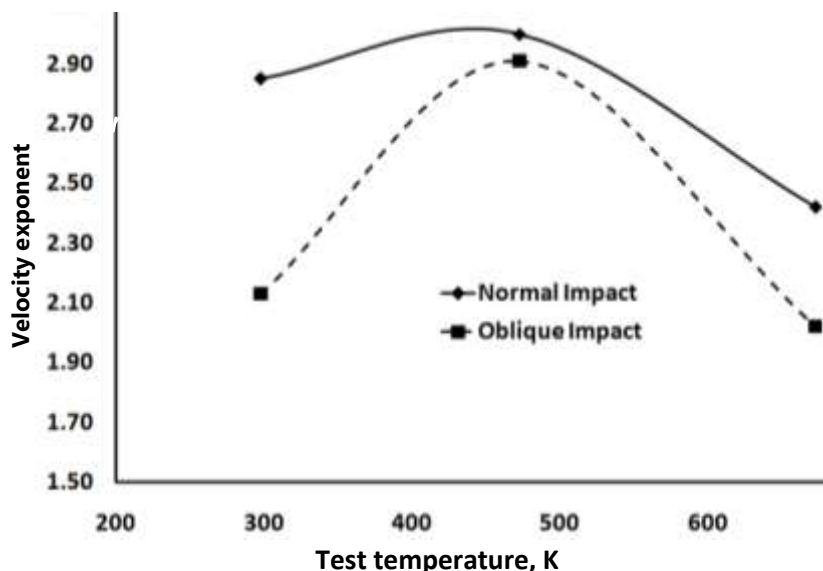

Figure 8. *The variation of velocity exponent* n *calculated for abradable coating as a function of test temperatures*

Morphology of eroded surfaces

Figure 9a shows the morphology of the surface of worn abradable coating at a 30° impact angle, at 93 m/s impact velocity, and ambient conditions. Material loss due to decohesion at the intersplat interface can be seen. No evidence of particle embodiment is noticed. Such features can be considered good in the sense that the embodiment of blade materials will be minimized during the operation of turbines, and coatings can perform their sealing action. Cracks were found to nucleate at the curled parts in the metallic matrix phase. The curled parts easily fall off under repeated impingement of impacting particles. This highlights the important role played by the micro-cutting and plowing due to the shear component of abrasive particles at a lower impact angle.
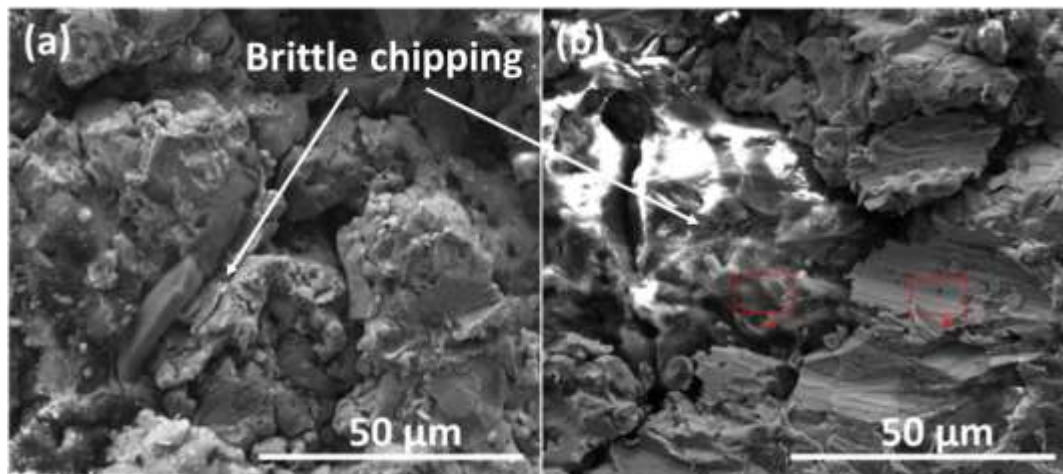

Figure 9. *SEM morphology of eroded coating tested at high velocity, oblique impact angle, and 673K temperature*
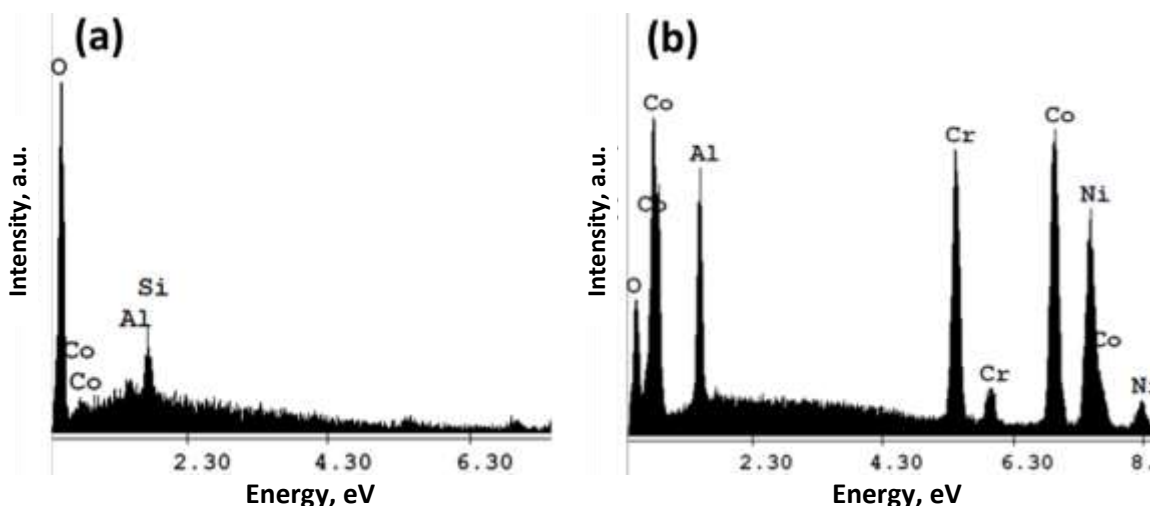
Figure 10. *EDS profile of eroded coating regions a and b in Figure 9 tested at high velocity, normal impact angle, and 673K temperature*

The SEM image of the eroded surface at oblique impact at high impact velocity and 673 K is presented in Figure 9b. The presence of formed curled parts, micro-cutting, and plowing traces are evident. The EDS profiles for the two regions marked in Figure 9 are shown in Figure 10, and this confirms the presence of an aluminum oxide scale on the surface. The presence of Si in EDS profiles in Fig. 10a confirms the presence of Si erodent particles embedded in the eroded surface, although Si embodiment is marginal. This also brings out the possibility of the formation of a kind of composite layer on the eroded surfaces [18,19]. The transverse section of the eroded abradable coating surfaces is illustrated in Figure 11. This also confirms inters plat decohesion as the main mechanism for materials loss, as noted in other thermal sprayed coatings [20]. This mechanism of materials removal from the thermal sprayed coating is different from what is normally observed for ductile materials, where the loss of material is generally caused by the formation of a lip and its subsequent fracture due to localization of deformation [21]. This mechanism is also different from brittle ceramic material, where material removal occurs by the formation of intersecting cone or radial cracks, nucleating from preexisting flaws once critical tensile stress is exceeded [22]. At this stage, it is pertinent to mention that the dimensionless erosion rate of CoNiCrAlY BN polyester abradable topcoat is comparable to that of YSZ thermal barrier coating (TBC) system under normal impact and lower than that of YSZ TBC system under oblique impact [23]. The erosion rate of YSZ thermal barrier coating (TBC) under normal and oblique impact were 1.62 and 0.57 g/ kg, respectively, at ambient conditions under high impact velocity. At lower impact velocity, the TBC system exhibits a lower erosion rate at all tested temperatures. The erosion rates of TBC at low impact velocity under normal and oblique are 0.36 and 0.20 mg/g respective at ambient conditions.

The comparable erosion rates of polymer containing abradable coating [24] and ceramic thermal barrier coating can be attributed to the deformation condition during erosion [25]. It can be noted that during erosion, the target material is indented by hard angular particles, as it happens during the hardness test. This leads to a multi-axial stress state. The thickness of the coating is significantly higher than the plastic zone size beneath the erodent. Thus, the plastic zone beneath the indenting erodent is totally confined. As a result, constrained plastic flow in the presence of hydrostatic compressive stresses can be realized. The estimated strain rates during erosion are in the range of 10^4 to 10^7 s^{-1}, which is ultrahigh strain rates. The eroding material can deform to large strains substantially higher than the tensile fracture strains prior to fracture during erosion. It is also demonstrated that the deformation during erosion is adiabatic. These above facts together

contribute towards unexpected erosion rates of polymer containing abradable coating and ceramic thermal barrier coating.
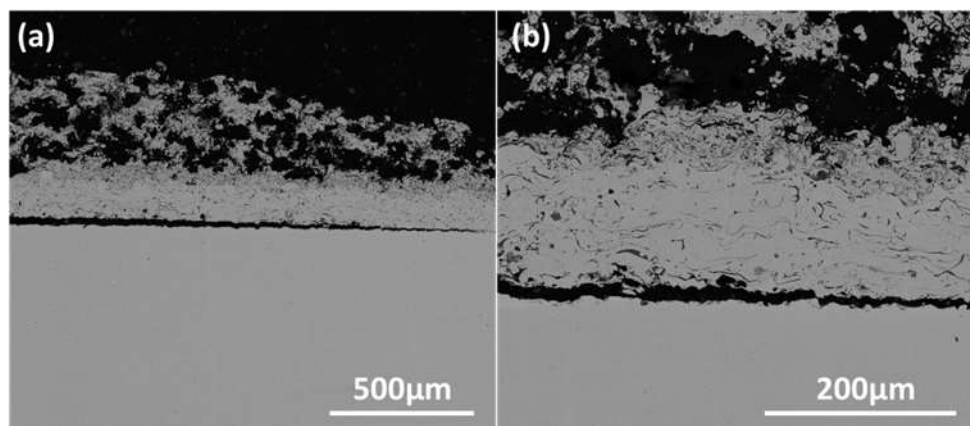

Figure 11. *Cross-sectional SEM micrographs of eroded abradable coating at different magnifications*

Conclusions

The erosion behavior of CoNiCrAlY BN polyester abradable coating has been evaluated as a function of erosion conditions up to 673 K. Main conclusions are:

1)   The erosion rate of CoNiCrAlY BN polyester abradable coating increases with an increase in temperature.

2)   This coating exhibits ductile erosion response at elevated temperature and at high impact velocity. This coating, however, responds in a brittle way at ambient conditions under high impact velocity.

3)   Detachment at the intersplat adhesion boundary is responsible for material loss.

4)   Velocity exponent is the maximum at intermediate temperature.

5)   Embodiment of erodent on the eroded surface is hardly noticed.

References

1.   Y. Cui, M. Guo, C. Wang, Z. Tang, L. Cheng, *Surface and Coatings Technology* **394** (2020) 125915. https://doi.org/10.1016/j.surfcoat.2020.125915

2.   S. Singh, K. Goyal, R. Bhatia, *Journal of Electrochemical Science and Engineering* **12(5)** (2022) 819-828. https://doi.org/10.5599/jese.1278

3.   M. Roy, J.P. Davim (Eds.), *Thermal Sprayed Coatings and their Tribological Properties*, IGI Global, 2015. https://doi.org/10.4018/978-1-4666-7489-9

4.   J. E. Jońca, B. Malard, J. Soulié, T. Sanviemvongsak, S. Selezneff, A. Vande Put, *Corrosion Science* **153** (2019) 170–177. https://doi.org/10.1016/j.corsci.2019.02.030

5.   X. M. Sun, L. Z. Du, H. Lan, H. F. Zhang, R. Y. Liu, Z. G. Wang, S. G. Fang, C. B. Huang, Z. A. Liu, W. G. Zhang, *Surface and Coatings Technology* **397** (2020) 126045. https://doi.org/10.1016/j.surfcoat.2020.126045

6.   M. Roy, M. Subramaniyam, G. Sundararajan, *Tribology International* **25** (1992) 271–280. https://doi.org/10.1016/0301-679X(92)90064-T

7.   M. Roy, K.K. Ray, G. Sundararajan, *Oxidation of Metals* **51** (1999) 251–272. https://doi.org/10.1023/A:1018870606617

8. Y. Maozhong, H. Baiyun, H. Jiawen, *Wear* **252** (2002) 9–15. https://doi.org/10.1016/S0043-1648(01)00681-0
9. M. Shadab Siddiqui, P. Joshi, N. Nayak, K. Vidyasagar, *Advanced Materials Letters* **5(9)** (2014) 506–510. https://doi.org/10.5185/amlett.2014.588
10. S. Sharsar, R. Bhagat, N. Kapoor, *International Journal of Research in Mechanical Engineering & Technology* **4** (2014) 4. http://www.ijrmet.com/vol4issue2/shekhar-sharsar.pdf
11. A. Kumar, Y. Sharma, S. Malik, *JRPS International Journal for Research Publication & Seminar* **05** (2014) 7.
12. M. Roy, *Transactions of the Indian Institute of Metals* **53** (2000) 623–638. https://www.researchgate.net/publication/285944502
13. A. W. Ruff, L.K. Ives, *Wear* **35** (1975) 195–199. https://doi.org/10.1016/0043-1648(75)90154-4
14. M. Roy, K. K. Ray, G. Sundararajan, *Metallurgical and Materials Transactions A* **32** (2001) 1431–1451. https://doi.org/10.1007/s11661-001-0232-5
15. M. Roy, *Journal of Thermal Spray Technology* **11** (2002) 393–399. https://doi.org/10.1361/105996302770348790
16. G. Sundararajan, P. G. Shewmon, *Wear* **84** (1983) 237–258. https://doi.org/10.1016/0043-1648(83)90266-1
17. M. Roy, Y. Tirupataiah, G. Sundararajan, *Materials Science and Technology* **11** (1995) 791–797. https://doi.org/10.1179/mst.1995.11.8.791
18. M. Roy, K. K. Ray, G. Sundararajan, *Wear* **217** (1998) 312–320. https://doi.org/10.1016/S0043-1648(98)00139-2
19. M. Roy, *Journal of Physics D* **39** (2006) R101–R124. https://doi.org/10.1088/0022-3727/39/6/R01
20. R. J. K. Wood, M. Roy, *Tribology of Thermal Sprayed Coating*, in: *Surface Engineering for Enhanced Performance against Wear*, M. Roy (Ed.), Springer, Vienna, 2013, pp. 1-43. https://doi.org/10.1007/978-3-7091-0101-8_1
21. M. Roy, Y. Tirupataiah, G. Sundararajan, *Materials Science and Engineering A* **165** (1993) 51–63. https://doi.org/10.1016/0921-5093(93)90626-P
22. S. G. Sapate, M. Roy, *Thermal Sprayed Coatings and Their Tribological Performances* (2015) 193–226. https://doi.org/10.4018/978-1-4666-7489-9.ch007
23. B. Malvi, M. Roy, *Journal of Thermal Spray Technology* **30** (2021) 1028–1037. https://doi.org/10.1007/s11666-021-01189-9
24. S. Sarkar, V.G. Sekharan, R. Mitra, M. Roy, *Tribology Transactions* **52(6)** (2009) 777-787. https://doi.org/10.1080/10402000903097411
25. P. Mukhopadhyay, M. Srinivas, M. Roy, *Materials Characterization* **113** (2016) 43–51. https://doi.org/10.1016/j.matchar.2016.01.008